Available online at www.sciencedirect.com
SCIENCE DIRECT®
Chemical Physics 289 (2003) 135–147
Chemical Physics
www.elsevier.com/locate/chemphys

Nuclear motion and symmetry breaking of the B 1s-excited BF_3 molecule

K. Ueda[a,*], A. De Fanis[a], N. Saito[b], M. Machida[c], K. Kubozuka[c], H. Chiba[a], Y. Muramatu[a], Y. Sato[a], A. Czasch[d], O. Jaguzki[d], R. Dörner[d], A. Cassimi[e], M. Kitajima[f], T. Furuta[f], H. Tanaka[f], S.L. Sorensen[g], K. Okada[h], S. Tanimoto[h], K. Ikejiri[h], Y. Tamenori[i], H. Ohashi[i], I. Koyano[c]

[a] *Institute of Multidisciplinary Research for Advanced Materials, Tohoku University, 2-1-1 Katahira, Aoba-ku, Sendai 980-8577, Japan*
[b] *National Metrology Institute of Japan, AIST, Tsukuba 305-8568, Japan*
[c] *Department of Material Science, Himeji Institute of Technology, Kamigori, Hyogo 678-1297, Japan*
[d] *Institut für Kernphysik, Universität Frankfurt, Frankfurt D-60486, Germany*
[e] *CIRIL/CEA/CNRS/ISMRA, University de Caen, Box 5133, F-14070 Caen Cedex 5, France*
[f] *Department of Physics, Sophia University, Tokyo 102-8554, Japan*
[g] *Institute of Physics, University of Lund, Box 118, Lund S-221 00, Sweden*
[h] *Department of Chemistry, Hiroshima University, Higashi-Hiroshima 739-8526, Japan*
[i] *SPring-8/Japan Synchrotron Radiation Research Institute, Sayo-gun, Hyogo 679-5198, Japan*

Received 28 February 2002

Abstract

Out-of-plane nuclear motion stimulated in the core-excited state and symmetry breaking due to this nuclear motion have been investigated for B 1s excitation in the BF_3 molecule by a combination of three different experimental methods: angle-resolved ion-yield spectroscopy, vibrationally resolved resonant Auger electron spectroscopy and quadruple-ion coincidence momentum-imaging technique.

1. Introduction

When a core electron of an atom in a molecule is excited, in general, the core hole relaxes by the Auger electron emission and ionic fragmentation proceeds along the dissociation path on the potential energy surface of the Auger-final state. The lifetime of the core-excited state for light atoms such as B, C, N, O and F is of the order of 10^{-15} s, i.e., femtoseconds (fs). Within this short time scale, however, nuclear motion of the molecule proceeds in the core-excited state in competition with the Auger decay [1–4].

We are particularly interested in core excitations of polyatomic molecules because of the following reasons. In the case of polyatomic

* Corresponding author. Tel.: +81-222175381; fax: +81-222175405.
E-mail address: ueda@tagen.tohoku.ac.jp (K. Ueda).

0301-0104/03/$ - see front matter
doi:10.1016/S0301-0104(02)00903-5

molecules, the symmetry of the stable geometry of the core-excited state is often different from that of the ground state [5–7] and as a result nuclear motion takes place towards a new stable geometry after the core excitation of the ground-state molecule. This nuclear motion induces the symmetry breaking and affects the subsequent electronic decay and ionic fragmentation processes. Thus one may be able to open up a new ionic fragmentation channel using the core excitation [8–10].

This paper is concerned with the core excitation of the BF_3 molecule. This molecule has a D_{3h} planar geometry in the ground state and its electronic configuration is

$$(\text{core})1a_1'^2 1e'^4 2a_1'^2 2e'^4 1a_2''^2 3e'^4 1e''^4 1a_2'^2; 2a_2''^0 4e'^0. \quad (1)$$

Here "(core)" includes F 1s and B 1s electrons. $1a_1'$ and $1e'$ are inner-valence orbitals whose character is mostly F 2s. The next six occupied orbitals are outer valence orbitals: $2a_1'$, $2e'$ and $1a_2''$ are bonding, $3e'$ and $1e''$ are slightly bonding having mostly F 2p character, whereas $1a_2'$ is non-bonding having pure F 2p character. The lowest unoccupied molecular orbital (LUMO) is $2a_2''$ having B $2p_z$ character and is non-bonding. The $4e'$ unoccupied molecular orbital has antibonding character and is located in energy above the ionization threshold forming a shape resonance.

There are four vibrational modes (v_1, v_2, v_3, v_4) in the ground state of the BF_3 molecule of D_{3h} symmetry; the symmetric stretching (breathing) mode v_1 of a_1' symmetry ($v_1 \sim 110$ meV), the out-of-plane bending mode v_2 of a_2'' symmetry ($v_2 \sim 89$ meV), the asymmetric stretching mode v_3 of e' symmetry ($v_3 \sim 186$ meV) and the asymmetric wagging mode v_4 of e' symmetry ($v_4 \sim 60$ meV) [11]. We expect the vibrational frequencies of these modes to change slightly from the ground state of the neutral to the core-ionized and core-to-Rydberg excited states of BF_3, due to the non-bonding character of the orbitals involved. Since v_3 and v_4 do not play a role in the present study, we consider only the v_1 and v_2 modes (v_1, v_2) throughout this paper unless indicated.

In the work described here, we focus on the excitation of the B 1s electron to the LUMO $2a_2''$. The B $1s^{-1}2a_2''$ core-excited state has a trigonometric pyramidal equilibrium geometry of C_{3v} symmetry [12]. Thus, after the core excitation, the central B atom is expected to go off transverse to the molecular plane determined by the three F atoms, towards the new equilibrium geometry. We investigate this out-of-plane nuclear motion (i.e., v_2 vibration of a_2'' symmetry), in relation to the ionic fragmentation after the Auger decay.

The experimental techniques employed here are angle-integrated (total) and angle-resolved ion-yield spectroscopy [13,14], subnatural-lifetime-width resonant Auger spectroscopy [15], and multiple-ion coincidence momentum-imaging technique [16]. The ion-yield spectra are recorded in the energy region not only for the B $1s \rightarrow 2a_2''$ excitation but also for the B $1s \rightarrow 3sa_1'$ excitation that arises as a result of vibronic coupling. The resonant Auger spectra are recorded at some energies across B $1s \rightarrow 2a_2''$ resonance and compared with the direct photoemission spectrum. The multiple-ion coincidence momentum-imaging spectra are recorded at the B $1s \rightarrow 2a_2''$ excitation and at the B $1s \rightarrow 4e'$ excitation above the B 1s ionization threshold.

The valence photoelectron spectrum of BF_3 was investigated by Haller et al. [17] Hagenow et al. [18] and by Shpinkova et al. [19]. The B 1s absorption spectrum of BF_3 was investigated by Ishiguro et al. [20]. The electronic decay after B $1s \rightarrow 2a_2''$ excitation was investigated by several groups [21–23]. The ionic fragmentation after B $1s \rightarrow 2a_2''$ excitation was investigated by means of various coincidence techniques such as resonant-Auger-electron–photoion coincidence (RAEPICO) [24,25] and photoelectron–photoion–photoion coincidence (PEPIPIC0) [12]. The structure of the B $1s^{-1}2a_2''$ state was investigated by means of ab initio self-consistent field calculations [12] and by means of vibronic-coupling model-potential calculations [23,26]. These extensive investigations provide us with a solid basis for designing the present dedicated experiments and for the analyses of the results.

2. Experiment

All the experiments are carried out on the c branch of the soft X-ray photochemistry beamline 27SU at SPring-8 [27]. A schematic diagram of the

c-branch of BL27SU and its end-stations for gas-phase experiments is presented in Fig. 1. The radiation source is a figure-8 undulator (a in Fig. 1) and provides linearly polarized light: the polarization vector E is horizontal for the first-order harmonic light and vertical for the 0.5th order harmonic light [28,29]. In the energy region of interest ($\sim$200 eV), however, one can use only 0.5th order harmonic light.

The monochromator installed in this branch (b in Fig. 1) is of Hettrick-type. It has three exchangable varied line-space plane gratings and covers the photon energy region between 150 eV and 2.5 keV [30]. The highest achievable resolutions are between 10,000 and 20,000, depending on energy. The photon band widths employed in the present experiments are 15–30 meV at $\sim$200 eV. Three exchangable focusing mirrors of different curvatures are placed in the mirror chamber (c in Fig. 1) and used to focus the photon beam into different experimental chambers, placed at three different positions.

The general-purpose chamber (d in Fig. 1) [31] contains the total ion-yield (TIY) detector (d_1 in Fig. 1) [13], aligned vertically. A pair of energetic-ion detectors (d_2 in Fig. 1) [14] are placed horizontally and vertically in the same chamber, 250 mm downstream of the TIY detector along the incident photon beam. The angle-resolved ion-yield curves for the energetic ions are measured by use of these ion detectors, with the retarding voltage set to $\sim$6 V.

The high-resolution electron spectroscopy apparatus (f in Fig. 1) is placed downstream of the general-purpose chamber. It consists of a hemispherical electron energy analyzer (SES2002 by Gammadata–Scienta), a gas cell and a differentially pumped main chamber [15]. The lens axis of the analyzer is in the horizontal direction and the entrance slit of the analyzer is set to be parallel to the photon beam direction. The whole system sits on an XYZ stage so that the focus point of the analyzer can be adjusted easily to the fixed photon beam position. The gas cell is operated at $\sim 10^{-3}$ Torr while the analyzer chamber is maintained at $\sim 10^{-6}$ Torr.

Resonant Auger spectra of BF_3 molecules are recorded under the conditions where the excitation photon band widths 15–30 meV are smaller than the natural lifetime width $\Gamma \sim 60$ meV of the B 1s core-excited state and the band width of the electron energy analyzer is set to approximately the same value of the photon band width. In this way we can record resonant Auger spectra whose overall widths are smaller than the natural lifetime width of the core-excited state [32,33]. Such measurements may be called *subnatural-lifetime-width resonant Auger spectroscopy*.

The high-resolution electron spectroscopy apparatus can be replaced by the multiple-ion coincidence momentum-imaging apparatus (e in Fig. 1). The momentum-imaging technique is based on the time-of-flight (TOF) method combined with a two-dimensional (2D) position-sensitive detector. Here,

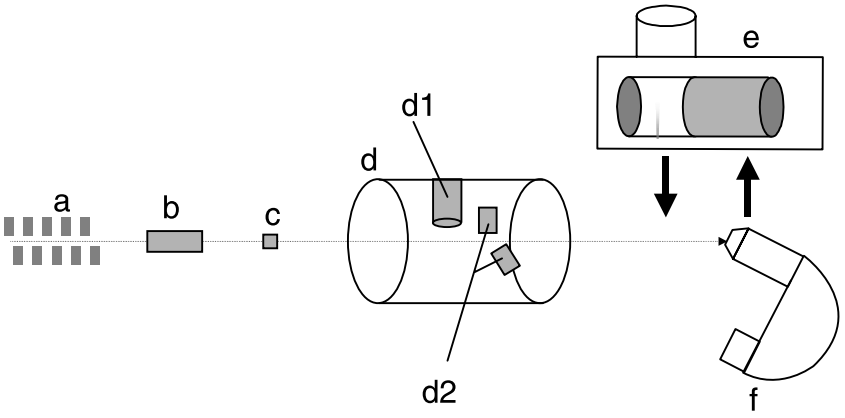

Fig. 1. Scheme of the experimental setup.

we consider the case where we detect all the four fragment ions produced from the quadruply charged parent ions BF_3^{4+} created after rapid multiple Auger decay. Complete registration of all the fragments allows one to extract all the kinematical information for the linear momentum (P_x, P_y, P_z) of each fragment ion without ambiguity.

In the momentum-imaging experiment, a BF_3 sample gas is introduced in the ionization point in the form of a supersonic jet and crosses the photon beam perpendicularly. The photon band width is set to ~30 meV. The TOF axis is fixed perpendicularly to both the light beam and the E vector of the incident light. The ion extraction field is ~20 V/mm, the length of the acceleration region is 71 mm, and the length of the drift region is about twice this value (i.e., 140 mm), so as to satisfy the space-focusing condition [34]. The TOF mass spectrometer is equipped with a multihit position-sensitive detector. It consists of micro-channel plates with effective diameter of 80 mm and a hexagonal-type delay-line anode (Hex80 by Roentdek [35]). This recently developed three-layer delay-line anode allows us to register positions and TOFs of more than two ions with the same mass (i.e., F^+ in the present experiment) in coincidence without suffering from the deadtime intrinsic to the conventional square delay-line anode.

3. Results and discussion

3.1. Total ion yields

Fig. 2 presents the TIY spectrum of BF_3 in the B 1s excitation region. We consider the TIY spectrum to be equivalent to the photoabsorption spectrum. The prominent broad band at 195.5 eV corresponds to the promotion of the B 1s electron to the LUMO $2a_2''$. The width of this band (FWHM) is ~250 meV, much larger than the expected natural lifetime width $\Gamma \sim 60$ meV and the excitation photon band width ~20 meV. It is not possible to resolve any vibrational structure. This is because the energy splitting among the vibronic levels is smaller than the natural lifetime width of the core-hole state.

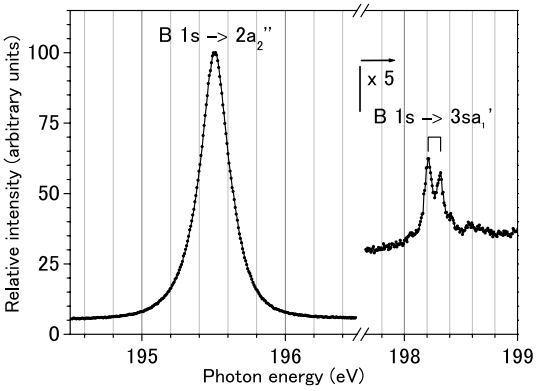

Fig. 2. The TIY spectrum of BF_3 in the B 1s excitation region.

The weak band at 198.2 eV corresponds to the B $1s \rightarrow 3sa_1'$ transition. This transition is electronically forbidden but it arises as a result of pseudo-Jahn–Teller vibronic coupling between the B $1s^{-1}2a_2''$ and B $1s^{-1}3sa_1'$ states via the out-of-plane v_2 vibrations of a_2'' symmetry. Vibrational structure is observable in this band. The energy splitting of the two prominent vibrational components is ~100 meV and corresponds to the frequency of the breathing vibrations v_1. The two prominent components are thus assigned to $(v_1, 1)$ with $v_1 = 0, 1$.

Tanaka et al. [26] analysed the absorption spectrum for these two bands, B $1s \rightarrow 2a_2''$ and B $1s \rightarrow 3sa_1'$, recorded with much larger photon band width [36], using the vibronic coupling model. In their analysis only the v_2 out-of-plane vibrational mode is taken into account and the matrix element of the pseudo-Jahn–Teller coupling between the B $1s^{-1}2a_2''$ and B $1s^{-1}3sa_1$ states is estimated in such a way to reproduce the intensity ratio of these two bands. Because of this coupling, the potential energy curves for the B $1s^{-1}2a_2''$ and $1s^{-1}3sa_1'$ states along the out-of-plane vibrational coordinate Q_2 strongly repel each other near the origin and thus the B $1s^{-1}2a_2''$ state becomes unstable at the origin. The calculation for the excitation from the ground state to the B $1s^{-1}2a_2''$ state predicted that many unresolved v_2 vibrational components form a slightly asymmetric band with a small tail toward lower energy, due to the negative sign of the the second-order derivative of the the potential energy curve at the origin. The

calculation for the B 1s → 3sa$'_1$ band on the other hand predicted that only one strong component (0, 1) appears. (Note that the model by Tanaka et al. does not include the ν_1 mode.) These predictions are in reasonable agreement even with the present high-resolution spectrum.

3.2. Angle-resolved ion yields

The angle-resolved ion-yield spectroscopy of fragment ions provides information about symmetries of inner-shell excited states of linear molecules [37–39], because the direction of the ion ejection relative to the polarization vector E reflects the direction of the dipole moment relative to the molecular axis. This type of measurements, called *symmetry-resolved absorption spectroscopy* [40–42], relies on the fact that the core-hole decay and fragmentation occur much faster than the molecular rotation, and thus the axial-recoil approximation [43,44] is valid. The extension of this technique to a planar molecule of D_{3h} symmetry is straightforward. If one assumes that the molecular fragmentation is within the molecular plane determined by the three F atoms, the values of the anisotropy parameter β of fragment ions are expected to be $\beta_{A''_2} = -1$ for the $A'_1 \rightarrow A''_2$ transition, in which the transition dipole moment is perpendicular to the molecular plane, and $\beta_{E'} = 0.5$ for the $A'_1 \rightarrow E'$ transition, in which the transition dipole moment is parallel to the molecular plane [45].

The lower panel of Fig. 3 presents the energetic ion yields $I(0)$ and $I(90)$ with kinetic energy larger than 6 eV recorded at 0° and 90° relative to the E vector. First we focus on the B 1s → 3sa$'_1$ band. The intensity of this band in $I(90)$ is much stronger than in $I(0)$, suggesting that the observed transition is $A'_1 \rightarrow A''_2$. This is consistent with the vibronic coupling picture in which the B 1s → 3sa$'_1$ transition becomes possible as a result of the intensity borrowing from the B 1s → 2a$''_2$ ($A'_1 \rightarrow A''_2$) transition [26]. The intensity of the B 1s → 3sa$'_1$ band in $I(0)$ is weak but still recognizable. This implies that there is a finite probability that the central B atom goes off transverse to the molecular plane by the weak bending motion ($v_2 = 1$) in the core-excited state and then the B^+ ion is ejected in the ionic fragmentation after the Auger decay having a small velocity component perpendicular to the molecular plane.

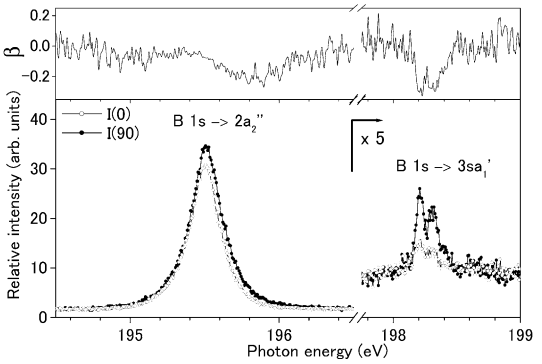

Fig. 3. Angle-resolved energetic ($KE > 6$ eV) ion-yield spectra of BF_3 in the B 1s excitation region, recorded at 0° and 90° relative to the E vector.

Now we focus on the B 1s → 2a$''_2$ band. Although this band arises from the $A'_1 \rightarrow A''_2$ transition, the intensity $I(0)$ is as significant as $I(90)$. The previous lower-resolution study illustrated that, at the B 1s → 2a$''_2$ excitation, the B^+ ion is ejected with large kinetic energy, having a significant velocity component perpendicular to the molecular plane, and as a result the symmetry resolution in the energetic ion-yield measurement is severely deteriorated [25]. The present high-resolution measurement is consistent with the the previous one and confirms the previous discussion [25].

The anisotropy parameter $\beta = 2[I(0) - I(90)]/[I(0) + 2 \times I(90)]$ is plotted in the upper panel of Fig. 3. The peak position of the B 1s → 2a$''_2$ resonance in $I(0)$ is slightly lower in energy than that in $I(90)$. As a result, the β value decreases from ∼−0.1 to ∼−0.3 when the energy increases across the B 1s → 2a$''_2$ band. This implies that, at lower excitation energy, there is a higher possibility of ejecting ions with large velocity components perpendicular to the molecular plane. A similar variation of β was also observed across the F 1s → 2a$''_2$ band of BF_3 [45].

Recall that similar variations of the β value across the band were also reported for the C/O 1s → 2π_u excitation bands in CO_2 [46,13]. In the case of the C/O 1s → 2π_u excitations in CO_2, there exist the overlapping linear and bent Renner–Teller pair states and the excitation ratio to the

linear and bent states changes as a function of energy across the band. This may partly explain the variation of β across the $1s \rightarrow 2\pi_u$ band. The B $1s^{-1}2a_2''$ state in BF_3 is, on the other hand, not degenerate and thus the variation of β across the band should be attributed to different samplings of the potential energy surface within a single electronic state.

The B $1s^{-1}2a_2''$ core-excited state has a C_{3v} trigonometric pyramidal equilibrium geometry, whereas the ground state has a D_{3h} planar equilibrium geometry. The excitation at lower energy thus corresponds to the creation of the wave packet at the nuclear coordinate where the B atom is more displaced from the plane. The wave packet then evolves in the B $1s^{-1}2a_2''$ state and the B atom goes off further transverse to the plane, in competition with the Auger decay. The Auger decay takes place mainly near the nuclear coordinate at the time of excitation (Condon point) because the natural lifetime ($\sim$10 fs) is shorter than the vibrational period ($\sim$50 fs). After the Auger decay, the ionic fragmentation takes place along the repulsive surface of the Auger final state. The observed variation of β suggests that, the more the B atom is out of the plane at the excitation, the more the B^+ ion receives the recoil momentum component transverse to the plane in the ionic fragmentation. This result may be a natural consequence of the ionic fragmentation (Coulomb explosion) that occurs reflecting the nuclear coordinate at the time when the ionization (i.e., the Auger decay) takes place.

In summary, based on the angle-resolved ion-yield spectra in the region of the B $1s \rightarrow 2a_2''$ excitation, we can infer that the out-of-plane nuclear motion proceeds in the core-excited state towards the new equilibrium geometry so that the B atom is out of the plane at the time of the Auger decay. The displacement of the B atom is however small, on average, relative to the distance to the outer turning point. Thus the displacement of the B atom at the time of the Auger decay still reflects the one at the time of excitation.

3.3. Electron emission

In order to confirm the competition between the nuclear motion and the Auger emission described in the previous section, in this section we investigate the Auger emission.

The Auger emission after the resonant excitation of the core electron to the unoccupied orbital is called *resonant Auger emission*. In the independent particle approximation, the resonant Auger emission is classified into two groups. If the excited electron participates in the Auger decay, the decay is called *participator Auger decay*. The final state of this decay is the same as that of the direct photoemission from the valence orbital and thus the participator Auger emission is observed as the resonance enhancement of the photoemission from the valence orbital. If the excited electron behaves as a spectator in the Auger decay, the decay is called *spectator Auger decay*. The spectator Auger decay is observed as the resonance enhancement of the satellite photoemission. The final states of the spectator Auger decay are two-hole one-particle in the valence orbitals. The aim of the present resonant photoemission investigation is to extract the information of the nuclear motion in the B $1s^{-1}2a_2''$ core-excited state in the BF_3 molecule. For this purpose, we focus on the vibrational structures observed in the participator Auger emission.

In Fig. 4(a), the electron emission spectrum recorded at the B $1s \rightarrow 2a_2''$ excitation is compared with the direct photoemission spectrum from the six valence orbitals $2a_1'$, $2e'$, $1a_2''$, $3e'$, $1e''$ and $1a_2'$. The photon and electron energy band widths employed are $\sim$15 meV for both. Vibrational structures are clearly resolved for the C $1a_2''^{-1}\,^2A_2''$, D $2e'^{-1}\,^2E'$ and E $2a_1'^{-1}\,^2A_1'$ emission bands. The electron emission for these bands, as well as for the B $3e'^{-1}\,^2E'$ band, is strongly enhanced by the B $1s \rightarrow 2a_2''$ excitation.

Focus on the C band. The enlarged spectrum of this band is shown in Fig. 4(b). Here the spectrum is plotted in binding energy scale relative to the $(0,0)$ component of the C band. The vibrational progression with the spacing of 96 meV observed in the direct photoemission is attributed to the ν_1 progression $(v_1,0)$ [17], as illustrated in the figure. Each vibrational component is strongly enhanced by the B $1s \rightarrow 2a_2''$ excitation. If the lifetimes of the core-excited state were practically zero, the photoemission band would be enhanced without change of vibrational distribution. The envelop of

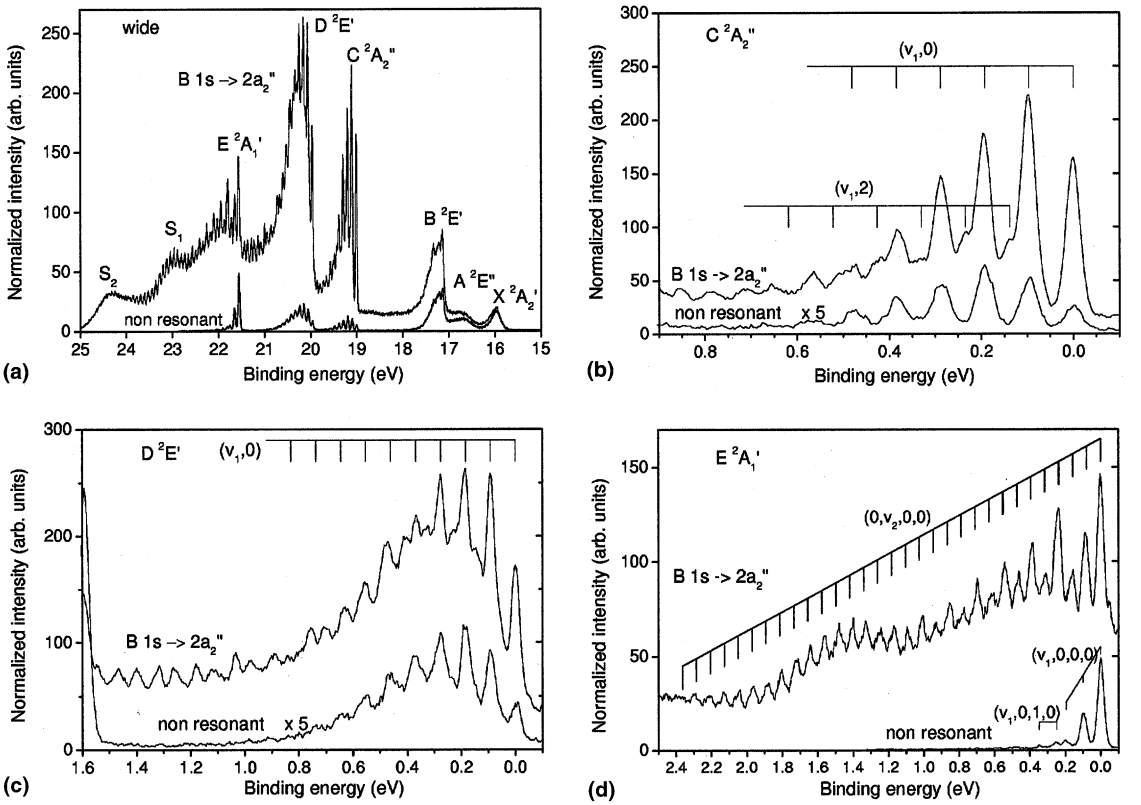

Fig. 4. Electron spectra of BF_3 corresponding to the emssion from the six outer valence orbitals. The resonant photoemission at the B $1s \rightarrow 2a_2''$ resonance is compared with the direct photoemission: (a) in the binding energy between 15 and 25 eV, (b) to the C^2A_2'' ionic state, (c) to the D^2E' ionic state and (d) to the E^2A_1' ionic state.

the $(v_1, 0)$ progression is however slightly modified by the B $1s \rightarrow 2a_2''$ excitation, suggesting that the nuclear motion proceeds slightly along the v_1 coordinate in the core-excited state. In the resonant photoemission spectrum, one can recognize additional vibrational progression which exhibits the peaks on the higher energy side of the $(v_1, 0)$ peaks with $v_1 \geqslant 1$. This progression may be attributed to the $(v_1, 2)$ progression ($v_2 \sim 80$ meV). The features which appear above 0.5 eV may be attributed to other vibrational components (v_1, v_2) but we face difficulties to identify the vibrational quanta, because the observed spacings are not regular and thus multimode vibronic couplings and Fermi resonances seem to play a role.

Focus on the D band. The enlarged spectrum of this band is shown in Fig. 4(c). The vibrational progresson with the spacing of 92 meV observed in the direct photoemission is attributed to $(v_1, 0)$ [17]. One may notice that there exist unresolved vibrational components between the revolved beaks. In the photoelectron spectrum excited by the He I radiation, one can recognize two additional progressions, descplanced from $(v_1, 0)$ by $\sim$60 and $\sim$40 meV [18,19]. One of them may be attributed to $(v_1, 0, 0, 1)$, with $v_4 \sim 60$ meV, which appears as a result of Jahn–Teller coupling [17], though the assignments are not conlusive [18,19]. In the resonant photoemission spectrum, besides strong enhancement for the members observed in the direct photoemission spectrum, one can recognize some additional vibrational components. It is clear that these components include excitation of the v_2 mode. However, we cannot give the definite assignments for the vibrational quantum numbers, because the observed spacings are quite irregular,

illustrating multimode vibronic couplings and Fermi resonances.

Focus on the E band. The enlarged spectrum of this band is shown in Fig. 4(d). The direct photoemission band was well characterized by Haller et al. [17]. The dominant progression with the spacing of 98 meV is $(v_1, 0, 0, 0)$: the intensity sharply drops with an increase in v_1. One can also recognize the weak progression $(v_1, 0, 1, 0)$ with $v_3 \sim 248$ meV. The second progression appears as a result of pseudo-Jahn–Teller coupling with the D state. In the resonant photoemission spectrum, one finds a well-extended vibrational progression. None of the vibrational components, besides $(0, 0, 0, 0)$, corresponds to the one observed in the direct photoemission and thus may be assigned to the $(0, v_2, 0, 0)$ progression. The spacings are in general regular, i.e., 79 ± 4 meV, whereas the intensity alters for the lower vibrational components.

In the previous moderate-resolution measurements [22,23], this vibrational progression was observed as continuous long tails without vibrational structures, because of the insufficient resolution employed. The extended vibrational progression was observed also by Miron et al. [47] with lower resolution than the present measurement. The extended vibrational progression is direct evidence that the Auger decay occurs while the wave packet evolves in the core-excited state and the nuclear motion proceeds. The nuclear motion we are probing here is the displacement of the B atom transverse to the molecular plane.

With the help of a classical picture, the extended vibrational progression can be interpreted as follows. The kinetic energy of the Auger electron corresponds to the energy difference of the adiabatic potentials between the core-excited and Auger final states. The Auger kinetic energy decreases while the B atom moves along the adiabatic potential curve in the out-of-plane direction in the B $1s^{-1}2a_2''$ core-excited state, because the core-excited state is unstable at the origin. Thus the Auger emission exhibits the tail towards the lower kinetic energy side, i.e., towards the higher binding energy side. This classical picture is fully supported by quantum calculations based on the vibronic coupling model [26]. The calculations indeed predicted a long progression of the v_2 out-of-plane vibrations towards the higher binding energy side of the photoemission band. The Auger emisson in competition with the nuclear motion in the core-excited state is called *dynamical Auger emission* [23,26].

Note that the calculations of Tanaka et al. were made within the simple model where only the v_2 mode is considered and furthermore the potential curves along the v_2 coordinate are assumed to be the same for the three Auger final states C, D and E. These oversimplifications prevent us from quantitative comparison of the calculations with the present high-resolution spectrum.

In the resonant photoemission spectrum of Fig. 4(a), there appears two satellite structures S_1 and S_2. Tanaka et al. [26] attributed the S_1 (S_2) satellite to the Auger emission around the point where the adiabatic potential energy curves of the B $1s^{-1}2a_2''$ core-excited state and the Auger final state $2e'^{-1}$ ($1a_2''^{-1}$) become parallel. The satellite structures originating from the parallelness between the two adiabatic potentials of the core-excited and Auger final states were observed also in the resonant Auger spectrum of the O_2 molecule [4]. If this is the case, the S_1 and S_2 satellites will remain at nearly constant kinetic energy even though the photon energy is scanned across the B $1s \rightarrow 2a_2''$ band, as demonstrated for O_2, because the kinetic energy corresponding to the satellite is determined by the energy difference between two adiabatic potentials of the core-excited and Auger final states where the potential curves become parallel.

In Figs. 5(a) and (b), we present the emission spectra in the vicinity of the S_1 and S_2 satellites excited by three different photon energies, in the binding and kinetic energy scales, respectively. The photon and electron energy band widths employed are $\sim$30 meV for both. The S_1 and S_2 satellites stay at nearly the same kinetic energies as seen in Fig. 5(b), independent of the excitation energies. This observation is consistent with the prediction by Tanaka et al. It should be noted that Miron et al. [47] found that these satellites move slightly by the larger change of excitation energy and thus attributed formation of these satellites to the outer-turning point effect. Further theoretical investigations are demanded to draw a decisive conclusion.

Finally, it may be worth to note the behaviors relative intensities of the vibrational components

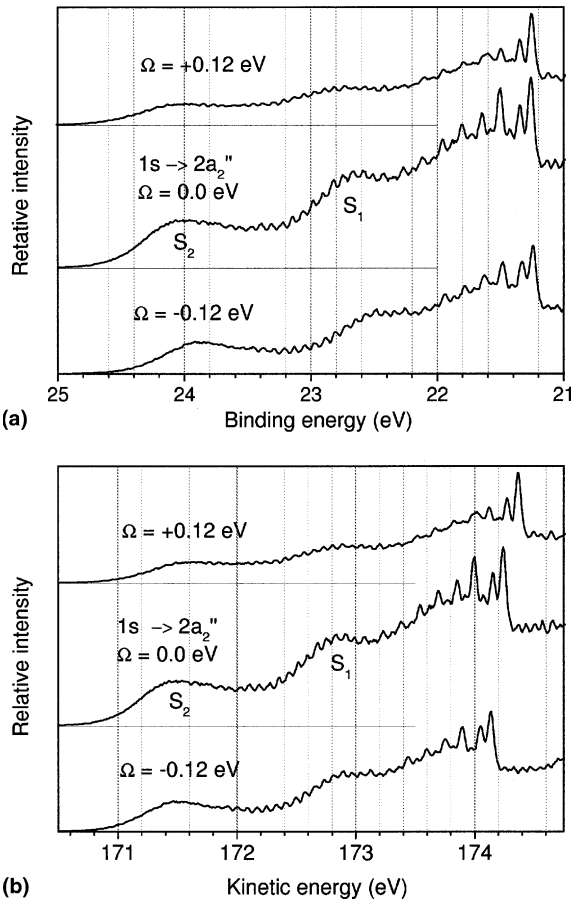

Fig. 5. Electron spectra corresponding to the resonant photoemission via the B $1s^{-1}2a_2''$ core-excited state, plotted against (a) binding energy and (b) kinetic energy. Ω is the difference between the excitation energy and the peak position of the B $1s \rightarrow 2a_2''$ resonance at 195.5 eV.

$(0, v_2)$ in the E band. In the on-resonant spectrum ($\Omega = 0$ eV) the relative intensity decreases with v_2 for the first three members ($(0, v_2)$ with $v_2 = 0, 1, 2$), whereas it alternates for the higher members ($v_2 > 2$). As one compares the spectra for positive ($\Omega = 0.12$ eV) and negative ($\Omega = -0.12$ eV) detuning, the relative intensities of the first three peaks are almost the same for positive and negative detuning, whereas those of the higher vibrational members are higher for negative detuning than for positive detuning. These behaviors cannot be explained with a simple model where only one vibrational mode v_2 in a single electronic state is taken into account, as introduced by Tanaka et al. [26].

In summary, the observed electron emission spectra fully supports the following picture. The out-of-plane nuclear motion proceeds in the B $1s^{-1}2a_2''$ core-excited state in competition with the Auger decay. The Auger decay occurs mostly near the Condon point where the excitation takes place. This results in the resonance enhancement of the vibrational components observed in the direct photoemission. The Auger decay occurring after the displacement of the B atom transverse to the molecular plane ends up with the long vibrational progression of the Auger final state. The observed emission spectra are qualitatively consistent with the predictions by Tanaka et al. In order to understand the detailed vibrational structures observed in the present high resolution resonant photoemission spectra, however, it is indispensable to take account of the multistate, multimode vibronic couplings, as well as interference effects between the discrete and continuum channels and among the vibrational components. Such theoretical studies are under considerations.

3.4. Multiple-ion coincidence momentum imaging

Both ion-yields and electron emission spectra strongly suggest that the out-of-plane v_2 nuclear motion is stimulated in the B $1s^{-1}2a_2''$ core-excited state. In this section, we illustrate how we could snapshot core-excited BF_3 molecule at the time of the Auger decay by use of the multiple-ion coincidence momentum-imaging technique.

The quadruply charged BF_3^{4+} molecular parent ion can be produced by the multiple Auger decay of the inner-shell excited or ionized states of BF_3. This channel is very weak, representing less than 1% of the total ionization yield. This quadruply charged molecular ion has high internal energy and breaks up very rapidly due to Coulomb explosion. Then the bond-rupture is simultaneous and the axial-recoil approximation [43,44] is valid. Thus, despite the small branching ratio to the formation of the quadruply charged BF_3^{4+} molecular parent ion, the vector correlation among the linear momenta of the four ions reflects the geometry of the core-excited molecule at the time

when the Auger decay takes place, because the properties of the excited state are independent of the decay channel. In order to snapshot the core-excited molecule at the time of the Auger decay, we examine the linear momenta of the fragments B^+ and three F^+ produced from the parent molecular ion BF_3^{4+}, measured in coincidence.

The vector correlation among the linear momenta of three particles produced by three-body break-up can be well represented by the Dalitz plots [48]. Fig. 6 helps to explain the way to construct the Dalitz plot. We introduce the normalized, squared momentum ϵ_i for each ion i,

$$\epsilon_i = \frac{|P_i|^2}{\sum_i |P_i|^2}, \tag{2}$$

where P_i is the linear momentum of the ion i, and define the Cartesian coordinates x_D and y_D as

$$x_D = \frac{\epsilon_2 - \epsilon_3}{3^{1/2}}, \quad y_D = \epsilon_1 - \frac{1}{3}. \tag{3}$$

Then all the data points (x, y) are within the circle in Fig. 6 and the distances from the data point (x, y) to the three sides of the regular triangle are ϵ_i.

In order to use the Dalitz plots for investigating the vector correlation among the four linear momenta of the four particles produced by the four-body break-up, we take the projection of the three linear momenta of the three particles to the plane perpendicular to the linear momentum of the remaining fourth particle. First consider the projections of the linear momenta of the three F^+ ions to the plane perpendicular to the linear momentum of the B^+ ion, i.e., the molecular plane, measured in coincidence. Fig. 7 presents the Dalitz plots for the projected linear momenta of the three F^+ ions thus defined. The upper one is recorded at the B 1s $\rightarrow$ 4e′ shape resonance above the B 1s ionization threshold, whereas the lower one is recorded at the B 1s $\rightarrow 2a_2''$ excitation. In both cases, most of the events are located near the central part of the Dalitz plots, suggesting that the linear momenta of the three F^+ ions have almost equal sizes and thus

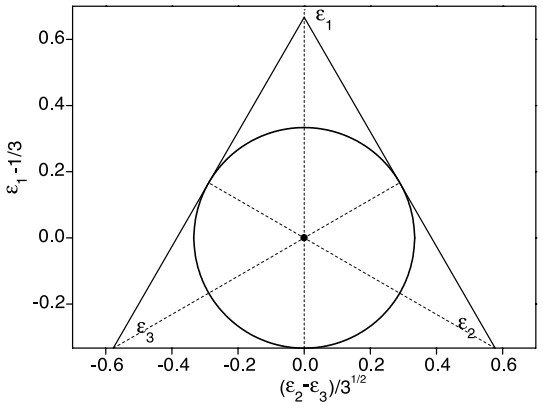

Fig. 6. Definition of the Dalitz plot (see text).

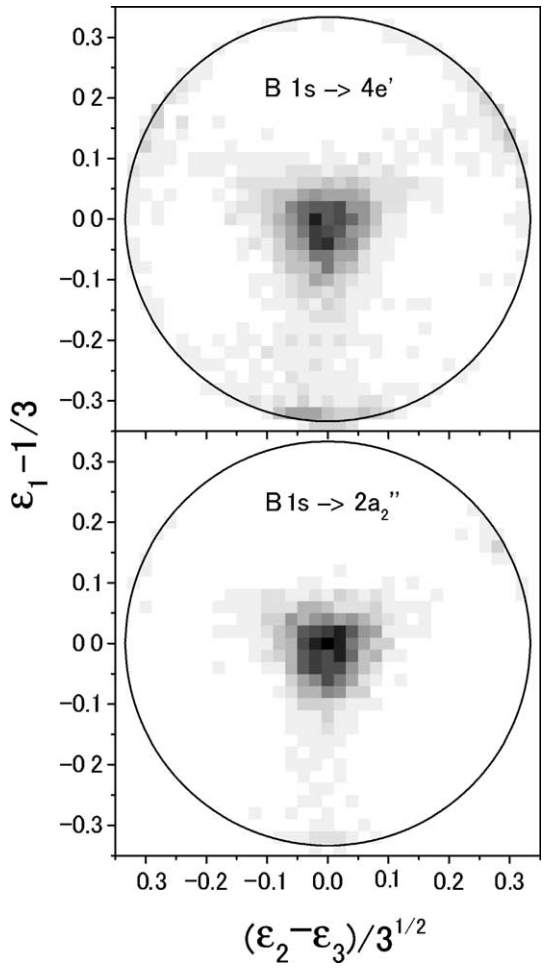

Fig. 7. Dalitz plots for the three F^+ fragments produced from BF_3^{4+}. Upper plot, recorded at the B 1s $\rightarrow$ 4e′ shape resonance. Lower plot, recorded at the B 1s $\rightarrow 2a_2''$ excitation. Projections are taken for the linear momenta of the three F^+ ions to the plane perpendicular the linear momentum of the B^+ ion, recorded in coincidence.

the rupture of the three B^+–F^+ bonds is simultaneous and symmetric.

One may notice that a fraction of data are located near the three radial axis. This is clear especially in the upper plot. These data points may perhaps reflect the sequential decay. Further detailed analysis is however demanded to draw the definite conclusion.

Now we investigate the expulsion of the B^+ fragment perpendicular to the molecular plane, in order to obtain evidence for the out-of-plane ν_2 molecular vibrations. Let us consider the projections of linear momenta of the B^+ ion and the two F^+ ions to the plane perpendicular to the linear momentum of the remaining F^+ ion. Fig. 8 presents the corresponding Dalitz plots recorded at the B $1s \rightarrow 4e'$ shape resonance and at the B $1s \rightarrow 2a_2''$ excitation. First we focus on the data in the upper panel, recorded at the B $1s \rightarrow 4e'$ shape resonance. Most of the data points are close to the bottom. This clearly indicates that the linear momentum of the B^+ ion is small and the ionic dissociation is mainly within the molecular plane. The non-zero component of the B^+ linear momentum is small but still finite. Even though the stable geometry of the B $1s^{-1}4e'$ state and of the B $1s^{-1}$ ionized state is planar, the B atom goes off slightly transverse to the molecular plane due to the zero-point ν_2 vibration. The Coulomb explosion enhances this small displacement, resulting in a non-negligible component of the linear momentum of the B^+ ion transverse to the molecular plane. Now we focus on the data in the lower panel, recorded at the B $1s \rightarrow 2a_2''$ excitation. It can be seen that the island at the bottom is elongated towards positive vertical axis and the intensity at the central part of the Dalitz plot is greatly enhanced, suggesting that the linear momentum of the B^+ ion is increased. We recall that the rupture of the three B^+–F^+ bonds is simultaneous and symmetric as seen in Fig. 7. Thus the increase in the B^+ linear momentum shown in Fig. 8 is a direct proof that the out-of-plane motion proceeds to a certain amount in the B $1s^{-1}2a_2''$ core-excited state before the Auger decay occurs.

In summary, we snapshot the BF_3 molecule at the time of the Auger decay, in the space of the linear momenta of the four fragment ions. The result fully confirms the physical picture derived on the basis of the ion-yields spectra and the electron emission spectra about the out-of-plane ν_2 vibrational motion proceeding in the B $1s^{-1}2a_2''$ state before the Auger decay occurs.

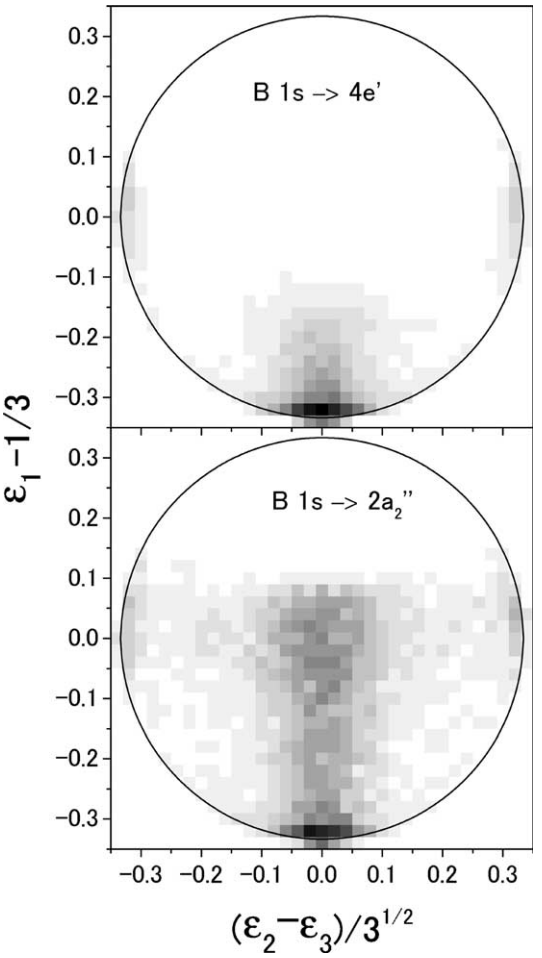

Fig. 8. Dalitz plots for the B^+ and two of the three F^+ fragments produced from BF_3^{4+}. Upper plot, recorded at the B $1s \rightarrow 4e'$ shape resonance. Lower plot, recorded at the B $1s \rightarrow 2a_2''$ excitation. Projections are taken for the linear momenta of B^+ and two F^+ to the plane perpendicular to the linear momentum of the remaining F^+ ion, recorded in coincidence.

4. Conclusion

We presented how the combination of three different experimental techniques, total and angle-resolved ion-yield spectroscopy, vibrationally

resolved resonant Auger spectroscopy and multiple-ion coincidence momentum-imaging technique, have been employed to investigate nuclear motion and symmetry breaking in the core-excited state. The results obtained by using different techniques fully support each other, and are also in agreement with theoretical predictions. The present work has focused on B $1s^{-1}2a_2''$ core-excited state of the BF_3 molecule, but the same investigation can be carried out for different excitations and other polyatomic molecules.

Acknowledgements

The experiments were carried out with the approval of the SPring-8 program advisory committee. KU and IK acknowledge financial supports by the Japan Society of the Promotion of Science (JSPS) in the form of Grants-in-Aid for Scientific Research, KU acknowledges further support by Matsuo Foundation, AD is grateful to JSPS for financial support, AC, OJ and RD acknowledge financial support by DFG and BMBF, RD acknowledges further support by the Heisenberg Programme der DFG and SLS is grateful to Swedish Foundation for Strategic Research (SSF) and Swedish Research Council (VR).

References

[1] M. Neeb, J.E. Rubensson, M. Biermann, W. Eberhardt, J. Electron Spectrosc. Relat. Phenom. 67 (1994) 261.
[2] S. Sundin, F.K. Gel'Mukhanov, H. Agren, S.J. Osborne, A. Kikas, O. Björneholm, A. Ausmees, S. Svensson, Phys. Rev. Lett. 79 (1997) 1451.
[3] I. Hjelte, M.N. Piancastelli, R.F. Fink, O. Björneholm, M. Bässler, R. Feifel, A. Giertz, H. Wang, K. Wiesner, A. Ausmees, C. Miron, S.L. Sorensen, S. Svensson, Chem. Phys. Lett. 334 (2001) 151.
[4] S.L. Sorensen, R. Fink, R. Feifel, M.N. Piancastelli, M. Bässler, C. Miron, H. Wang, I. Hjelte, O. Björneholm, S. Svensson, Phys. Rev. A 64 (2001) 012719.
[5] T. Lebrun, M. Lavollée, M. Simon, P. Morin, J. Chem. Phys. 98 (1993) 2534.
[6] J. Adachi, N. Kosugi, E. Shigemasa, A. Yagishita, J. Chem. Phys. 102 (1995) 7369.
[7] K. Ueda, S. Tanaka, Y. Shimizu, Y. Muramatsu, H. Chiba, T. Hayaishi, M. Kitajima, H. Tanaka, Phys. Rev. Lett. 85 (2000) 3129.
[8] K. Ueda, M. Simon, C. Miron, N. Leclercq, R. Guillemin, P. Morin, S. Tanaka, Phys. Rev. Lett. 83 (1999) 3800.
[9] P. Morin, M. Simon, C. Miron, N. Leclercq, E. Kukk, J.D. Bozek, N. Berrah, Phys. Rev. A 61 (2000) 050701.
[10] A. Hiraya, K. Nobusada, M. Simon, K. Okada, T. Tokushima, Y. Senba, H. Yoshida, K. Kamimori, H. Okumura, Y. Shimizu, A.-L. Thomas, P. Millie, I. Koyano, K. Ueda, Phys. Rev. A 63 (2001) 042705.
[11] T. Shimanouchi, in: Tables of Molecular Vibrational Frequencies Consolidated, Volume II, J. Phys. Chem. Ref. Data 6 (3) (1972) 993.
[12] M. Simon, P. Morin, P. Lablanquie, M. Lavollee, K. Ueda, N. Kosugi, Chem. Phys. Lett. 238 (1995) 42.
[13] N. Saito, K. Ueda, M. Simon, K. Okada, Y. Shimizu, H. Chiba, Y. Senba, H. Okumura, H. Ohashi, Y. Tamenori, S. Nagaoka, A. Hiraya, H. Yoshida, E. Ishiguro, T. Ibuki, I.H. Suzuki, I. Koyano, Phys. Rev. A 62 (2000) 042503.
[14] K. Ueda, H. Yoshida, Y. Senba, K. Okada, Y. Shimizu, H. Chiba, H. Ohashi, Y. Tamenori, H. Okumura, N. Saito, S. Nagaoka, A. Hiraya, E. Ishiguro, T. Ibuki, I.H. Suzuki, I. Koyano, Nucl. Instr. Meth. A 467–468 (2001) 1502.
[15] Y. Shimizu, H. Ohashi, Y. Tamenori, Y. Muramatsu, H. Yoshida, K. Okada, N. Saito, H. Tanaka, I. Koyano, S. Shin, K. Ueda, J. Electron Spectrosc. Relat. Phenom. 63 (2001) 114.
[16] Y. Muramatsu, K. Ueda, N. Saito, H. Chiba, M. Lavollée, A. Czasch, T. Weber, O. Jagutzki, H. Schmidt-Böcking, R. Moshammer, U. Becker, K. Kubozuka, I. Koyano, Phys. Rev. Lett. 88 (2002) 133002.
[17] E. Haller, H. Köppel, L.S. Cederbaum, W. von Nisessen, G. Bieri, J. Chem. Phys. 78 (1983) 1359.
[18] G. Hagenow, K. Hottmann, H. Baumgärtel, Chem. Phys. Lett. 164 (1989) 395.
[19] L.G. Shpinkova, D.M. Holland, D.A. Shaw, Mol. Phys. 96 (1999) 323.
[20] E. Ishiguro, S. Iwata, T. Suzuki, A. Mikuni, T. Sasaki, J. Phys. B 15 (1982) 1841.
[21] H. Kanamori, S. Iwata, A. Mikuni, T. Sasaki, J. Phys. B 17 (1984) 3887.
[22] K. Ueda, H. .Chiba, Y. Sato, T. Hayaishi, E. Shigemasa, Y. Yagishita, J. Chem. Phys. 101 (1994) 3520.
[23] M. Simon, C. Miron, N. Leclercq, P. Morin, K. Ueda, Y. Sato, S. Tanaka, Y. Kayanuma, Phys. Rev. Lett. 79 (1997) 3857.
[24] K. Ueda, H. Chiba, Y. Sato, T. Hayaishi, E. Shigemasa, Y. Yagishita, Phys. Rev. A 46 (1992) R5.
[25] K. Ueda, K. Ohmori, M. Okunishi, H. Chiba, Y. Shimizu, Y. Sato, T. Hayaishi, E. Shigemasa, A. Yagishita, Phys. Rev. A 52 (1995) R1815.
[26] S. Tanaka, Y. Kayanuma, K. Ueda, Phys. Rev. A 57 (1998) 3437.
[27] H. Ohashi, E. Ishiguro, Y. Tamenori, H. Kishimoto, M. Tanaka, M. Irie, T. Ishikawa, Nucl. Instr. Meth. A 467–468 (2001) 529.
[28] T. Tanaka, H. Kitamura, Nucl. Instr. Meth. A 364 (1995) 368.

[29] T. Tanaka, H. Kitamura, J. Synchrotron Radiat. 3 (1996) 47.
[30] H. Ohashi, E. Ishiguro, Y. Tamenori, H. Okumura, A. Hiraya, H. Yoshida, Y. Senba, K. Okada, N. Saito, I.H. Suzuki, K. Ueda, T. Ibuki, S. Nagaoka, I. Koyano, T. Ishikawa, Nucl. Instr. Meth. A 467–468 (2001) 533.
[31] I. Koyano, M. Okuyama, E. Ishiguro, A. Hiraya, H. Ohashi, T. Kanashima, K. Ueda, I.H. Suzuki, T. Ibuki, J. Synchrotron Radiat. 5 (1998) 545.
[32] A. Kivimäki, A. Naves de Brito, S. Aksela, S. Aksela, H. Aksela, O.-P. Sairanen, A. Ausmees, S.J. Osborne, L.B. Dantas, S. Svensson, Phys. Rev. Lett. 71 (1993) 4307.
[33] T. Åberg, B. Crasemann, in: G. Materlik, C.J. Sparks, K. Fischer (Eds.), Resonant Anomalous X-Ray Scattering, North-Holland, Amsterdam, 1994.
[34] W.C. Wiley, I.H. McLaren, Rev. Sci. Instrum. 26 (1955) 1150.
[35] See www.Roentdek.com for details of the detectors.
[36] K. Ueda, in: A. Yagishita, T. Sasaki (Eds.), Atomic and Molecular Photoionization (Proccedings of Oji International Seminar), Universal Academy press, Tokyo, 1996, p. 139.
[37] N. Saito, I.H. Suzuki, Phys. Rev. Lett. 61 (1988) 2740.
[38] A. Yagishita, H. Maezawa, M. Ukai, E. Shigemasa, Phys. Rev. Lett. 62 (1989) 36.
[39] K. Lee, D.Y. Lim, C.I. Ma, D.A. Lapiano-Smith, D.M. Manson, J. Chem. Phys. 93 (1990) 7936.
[40] E. Shigemasa, K. Ueda, Y. Sato, T. Sasaki, A. Yagishita, Phys. Rev. A 45 (1992) 2915.
[41] A. Yagishita, E. Shigemasa, J. Adachi, N. Kosugi, in: F.J. Weuillemier, Y. Petroff, I. Nenner (Eds.), Proceedings of the 10th International Conference on Vacuum Ultraviolet Radiation Physics, World Scientific, Singapore, 1996, p. 201.
[42] N. Kosugi, J. Electron Spectrosc. Relat. Phenom. 79 (1996) 351.
[43] R.N. Zare, Mol. Photochem. 4 (1972) 1.
[44] G.E. Busch, K.R. Wilson, J. Chem. Phys. 56 (1972) 3638.
[45] Y. Shimizu, K. Ueda, H. Chiba, M. Okunishi, K. Ohmori, J.B. West, Y. Sato, J. Chem. Phys. 107 (1997) 2419.
[46] J. Adachi, N. Kosugi, E. Shigemasa, A. Yagishita, J. Chem. Phys. 107 (1997) 4919.
[47] C. Miron, R. Feifel, O. Björneholm, S. Svensson, A. Naves de Brito, S.L. Sorencen, M.N. Piancastelli, M. Simon, P. Morin, Chem. Phys. Lett. 359 (2002) 48.
[48] R.H. Dalitz, Philos. Mag. 44 (1953) 1068.